Neuroinflammatory Component of Gray Matter Pathology in Multiple Sclerosis

Elena Herranz, PhD,[1,2] Costanza Giannì, MD,[1,2] Céline Louapre, MD, PhD,[1,2] Constantina A. Treaba, MD, PhD,[1,2] Sindhuja T. Govindarajan, MS,[1] Russell Ouellette, BSc,[1] Marco L. Loggia, PhD,[1,2] Jacob A. Sloane, MD,[2,3] Nancy Madigan, PhD,[2,3] David Izquierdo-Garcia, PhD,[1,2] Noreen Ward, MS,[1] Gabriel Mangeat, MS,[1,4] Tobias Granberg, MD, PhD,[1,2] Eric C. Klawiter, MD,[2,5] Ciprian Catana, MD, PhD,[1,2] Jacob M. Hooker, PhD,[1,2] Norman Taylor, MD,[2,6] Carolina Ionete, MD, PhD,[7] Revere P. Kinkel, MD,[3,8] and Caterina Mainero, MD, PhD[1,2]

Objective: In multiple sclerosis (MS), using simultaneous magnetic resonance–positron emission tomography (MR-PET) imaging with ^{11}C-PBR28, we quantified expression of the 18kDa translocator protein (TSPO), a marker of activated microglia/macrophages, in cortex, cortical lesions, deep gray matter (GM), white matter (WM) lesions, and normal-appearing WM (NAWM) to investigate the in vivo pathological and clinical relevance of neuroinflammation.
Methods: Fifteen secondary-progressive MS (SPMS) patients, 12 relapsing–remitting MS (RRMS) patients, and 14 matched healthy controls underwent ^{11}C-PBR28 MR-PET. MS subjects underwent 7T T_2^*-weighted imaging for cortical lesion segmentation, and neurological and cognitive evaluation. ^{11}C-PBR28 binding was measured using normalized 60- to 90-minute standardized uptake values and volume of distribution ratios.
Results: Relative to controls, MS subjects exhibited abnormally high ^{11}C-PBR28 binding across the brain, the greatest increases being in cortex and cortical lesions, thalamus, hippocampus, and NAWM. MS WM lesions showed relatively modest TSPO increases. With the exception of cortical lesions, where TSPO expression was similar, ^{11}C-PBR28 uptake across the brain was greater in SPMS than in RRMS. In MS, increased ^{11}C-PBR28 binding in cortex, deep GM, and NAWM correlated with neurological disability and impaired cognitive performance; cortical thinning correlated with increased thalamic TSPO levels.
Interpretation: In MS, neuroinflammation is present in the cortex, cortical lesions, deep GM, and NAWM, is closely linked to poor clinical outcome, and is at least partly linked to neurodegeneration. Distinct inflammatory-mediated factors may underlie accumulation of cortical and WM lesions. Quantification of TSPO levels in MS could prove to be a sensitive tool for evaluating in vivo the inflammatory component of GM pathology, particularly in cortical lesions.

ANN NEUROL 2016;00:000–000

Demyelinated cortical lesions and diffuse cortical and deep gray matter (GM) degeneration are established components of multiple sclerosis (MS) pathology, and major substrates of disease progression.[1]

The pathophysiological mechanisms leading to cortical and deep GM degeneration in MS are unknown. Early neuropathological descriptions of MS cortical lesions suggested that the histopathological and

View this article online at wileyonlinelibrary.com. DOI: 10.1002/ana.24791

Received Feb 29, 2016, and in revised form Sep 7, 2016. Accepted for publication Sep 25, 2016.

Address correspondence to Dr Mainero, A. A. Martinos Center for Biomedical Imaging, Building 149, Thirteenth Street, Charlestown, MA 02129. E-mail: caterina@nmr.mgh.harvard.edu

From the [1]Athinoula A. Martinos Center for Biomedical Imaging, Department of Radiology, Massachusetts General Hospital, Boston, MA; [2]Harvard Medical School, Boston, MA; [3]Department of Neurology, Beth Israel Deaconess Medical Center, Boston, MA; [4]Institute of Biomedical Engineering, Montreal Polytechnic, Montreal, Quebec, Canada; [5]Department of Neurology, Massachusetts General Hospital, Boston, MA; [6]Department of Anesthesiology, Massachusetts General Hospital, Boston, MA; [7]UMass Multiple Sclerosis Medical Center, Worcester, MA; and [8]University of San Diego, San Diego, California.

immunopathological characteristics of cortical demyelination differ significantly from those in white matter (WM), based on the evidence that cortical lesions lacked the inflammatory pattern typical of WM plaques.[2,3] Subsequent pathological examinations, however, suggested that cortical MS lesions might develop following meningeal inflammation accompanied by cortical microglia activation.[4,5] The role of activated microglia in cortical MS lesion pathogenesis is not without controversies, and is not uniformly observed.[6] Nevertheless, postmortem studies demonstrate that severe cortical microglia activation and demyelination are associated with a less favorable disease outcome.[4–6]

Activation of microglia/macrophages, associated with demyelination and neurodegeneration, has been pathologically observed in deep GM[7] and hippocampus in MS,[8,9] although their exact pathophysiologic role and clinical implications remain unclear.

The in vivo study of microglia/macrophage activation in the cortex, particularly cortical lesions, and deep GM could elucidate the role of neuroinflammation in the pathogenesis of demyelination and neurodegeneration of these structures, as they usually lack the blood–brain barrier abnormalities commonly detected in WM lesions using gadolinium magnetic resonance imaging (MRI).[10,11] Additionally, activated microglia/macrophages can be present even in the absence of the blood–brain barrier disruption seen on contrast-enhanced MRI.[12]

Activated microglia/macrophages upregulate expression of the 18kDa translocator protein (TSPO), which can be imaged in vivo by selective positron emission tomography (PET) TSPO radioligands, of which ^{11}C-PK11195 is the best known.[13] In MS, ^{11}C-PK11195 studies have reported increased TSPO levels in the cortex,[14] thalamus,[15] and central deep GM[16]; however, knowledge of microglia/macrophage activation in MS cortical lesions is still lacking due to the low sensitivity of clinical imaging tools to detect cortical demyelination. Seven-tesla (7T) T_2^*-weighted gradient-echo protocols demonstrate increased sensitivity to in vivo visualization of focal cortical lesions in MS, confirmed pathologically to correspond to cortical areas with the greatest degree of demyelination.[17,18]

^{11}C-PBR28 is a second-generation TSPO PET tracer[19] with ~80 times more specific binding than ^{11}C-PK11195[20] and good reproducibility.[21] In experimental studies, inflammation-induced microglial activation determined ^{11}C-PBR28 signal increase, confirmed pathologically to mainly result from microglia binding.[22]

We combined ^{11}C-PBR28 imaging on an integrated 3T magnetic resonance (MR)-PET system with 7T T_2^*-weighted MRI to quantify, in a heterogeneous MS cohort, microglia/macrophage activation in the (1) cortex, particularly in cortical lesions segmented at 7T; and (2) thalamus, basal ganglia, and hippocampus.

We investigated the relationship between ^{11}C-PBR28 uptake in the cortex and deep GM and neurological disability, cognition, and structural MRI metrics of neurodegeneration, to better understand the prevailing effects of neuroinflammation in MS, whether mainly harmful or beneficial. Finally, we quantified ^{11}C-PBR28 uptake in lesional and normal-appearing WM (NAWM) to investigate their MRI and clinical correlates, and to assess whether similar levels of TSPO expression could be detected in lesional tissue in the cortex and WM.

Subjects and Methods

Subjects

The institutional review board and the Radioactive Drug Research Committee approved all study procedures, and subjects gave written informed consent to participate in the study.

Twenty-seven MS subjects (15 secondary-progressive MS [SPMS], 12 relapsing–remitting MS [RRMS]) were prospectively enrolled from 33 MS subjects who were genotyped for the *TSPO* gene Ala147Thr polymorphism, which predicts binding affinity to ^{11}C-PBR28.[23] Only high- and mixed-affinity binders underwent subsequent study procedures. Fourteen age-matched and TSPO affinity binding–matched healthy individuals were included as controls. Inclusion criteria were: age between 18 and 65 years, a diagnosis of clinically definite MS, education ≥ 8 years, absence of clinical relapse within 3 months, no use of corticosteroids within 1 month of study enrollment, and being on stable disease-modifying treatment or no treatment for at least 6 months. Exclusion criteria were: treatment with benzodiazepines and blood thinners, general PET/MRI contraindications, and major medical and/or psychiatric disorders. In MS, major depression was excluded using the Beck Depression Inventory–II (cutoff score > 28).

In MS subjects, within 1 week from imaging procedures, neurological disability was assessed using the Expanded Disability Status Scale (EDSS),[24] and cognitive performance with the following tests: Symbol Digit Modalities Test (SDMT), Trail Making Test (Trails A and B), California Verbal Learning Test–II (CVLT-II), Brief Visuospatial Memory Test–Revised (BVMT-R), and Wisconsin Card Sorting Test–64 Card Version (WCST). For each patient, a z score was calculated to assess information-processing speed (average SDMT and Trails A z scores), and executive (average WCST and Trails B z scores) and memory (average CVLT-II and BVMT-R z scores) functions.

Imaging Data Acquisition

All subjects underwent a 90-minute ^{11}C-PBR28 MR-PET scan on a Siemens (Erlangen, Germany) simultaneous MR-PET system, BrainPET, a brain PET scanner operating in the bore of a

3T whole-body MR system equipped with an 8-channel head coil.[25] The spatial resolution of the BrainPET (<3mm in the center of the field of view) is superior to that of any other whole-body PET scanner, because of the smaller size of scintillator crystals and of the scanner diameter, which minimizes the noncolinearity effect.[26] Within 1 week from MR-PET, 24 MS subjects underwent 7T MRI on a Siemens scanner using a 32-channel head coil. Three subjects were excluded due to the presence of implants not approved for 7T.

MR-PET ACQUISITION. All participants received an intravenous bolus injection of ^{11}C-PBR28 produced in-house.[27] The mean ± standard deviation (SD) administrated dose was 11.4 ± 0.7mCi in MS and 11.7 ± 0.5mCi in controls. PET data were acquired in list-mode format during the 90-minute scan. In 15 MS subjects (10 SPMS, 5 RRMS) and 11 controls, blood data were sampled from an arterial line during the 90-minute PET acquisition (2ml every 6 seconds during the first 3 minutes and at 5, 10, 20, 30, 60, and 90 minutes postinjection) to generate an arterial plasma input function. Plasma metabolite analysis was performed as previously outlined.[28] In the remaining subjects, blood data were not collected either because subjects preferred not to undergo arterial line placement (n = 13) or because an anesthesiologist was not available during PET (n = 2).

MRI scans acquired simultaneously during PET included: (1) multiple gradient echo 3-dimensional (3D) magnetization-prepared rapid acquisition (ME-MPRAGE) images (1mm isotropic voxels)[29] for cortical surface reconstruction, coregistration to PET/7T data, segmentation of deep GM, and generation of attenuation correction maps[30]; (2) conventional 3D fluid-attenuated inversion recovery (FLAIR) images (1mm isotropic voxels) for WM lesion segmentation; and (3) diffusion images (60 diffusion-encoding directions, b value = 3,000s/mm^2, 8 volumes without diffusion weighting, 2.5mm isotropic voxels) for assessing microstructural integrity in the pseudoreference region used for normalizing PET data. In 9 patients, ME-MPRAGE and FLAIR images were acquired after administration of a single dose (0.1mmol/kg) of gadolinium.

7T MRI ACQUISITION. The 7T protocol included acquisition of 2D fast low-angle shot-T_2^* spoiled single-echo and/or multiecho images covering the supratentorial brain ($0.33 \times 0.33 \times 1$mm^3 voxels, 25% gap) for cortical lesion segmentation as previously detailed.[18]

MRI Data Analysis

LESION SEGMENTATION. White matter lesions were segmented on FLAIR images using a semiautomated method (3D Slicer v4.2.0), and lesion volume was computed using FSL (http://fsl.fmrib.ox.ac.uk/fsl/fslwiki/FSL).

Using Slicer, 2 raters, blinded to patients' demographic/clinical data, segmented by consensus on 7T T_2^*-weighted magnitude images (either from single-echo scans or, in those cases with motion artifacts in single-echo scans, from an average high-contrast image from multiecho acquisitions) (1) focal intracortical lesions and (2) leukocortical lesions, as previously detailed,[18] and defined as focal cortical hyperintensities extending over at least 3 voxels across 2 consecutive slices.

No foci of enhancement were observed in either WM or GM in patients on postgadolinium scans during MR-PET.

CORTICAL AND SUBCORTICAL GM SEGMENTATION. Pial and WM surface reconstruction and cortical thickness estimation were performed using FreeSurfer (v5.3.0, http://surfer.nmr.mgh.harvard.edu) on the 3D ME-MPRAGE volume, the recommended anatomical sequence for FreeSurfer.[29] Topological defects in cortical surfaces due to lesions in WM and cortex were corrected with lesion in-painting.

Automated segmentation of deep GM (thalamus, hippocampus, basal ganglia) was performed using FIRST/FSL, and deep GM fractions were obtained by dividing each volume by the total intracranial volume in FreeSurfer.

DIFFUSION IMAGING DATA. Diffusion MR images were processed using FSL/FMRIB's Diffusion Toolbox according to the following steps: (1) alignment of all images in the series to the first non–diffusion-weighted image using affine registration, (2) eddy current correction, and (3) fitting of the diffusion tensor model at each voxel. Mean diffusivity maps were obtained in each subject.

Quantification of ^{11}C-PBR28 Binding

In all subjects, ^{11}C-PBR28 binding was assessed across brain regions using standardized uptake values (SUV) normalized by a pseudoreference region. In 15 MS and 11 controls, we also quantified ^{11}C-PBR28 volume of distribution (V_T) using a 2-tissue compartment model with a metabolite-corrected arterial plasma curve as the input function.

^{11}C-PBR28 SUV. In-house software was used to compute voxelwise, for each subject, SUV (mean radioactivity/injected dose/weight) from the 60- to 90-minute postinjection data following a 2-step process. A preliminary SUV image was created using an attenuation correction map computed from the ME-MPRAGE in its native space.[30] To account for possible motion between the time the ME-MPRAGE and the 60- to 90-minute PET data were acquired, the ME-MPRAGE was coregistered to this preliminary image using SPM8. The resulting transformation matrix was applied to move the attenuation map into the final PET space. A final SUV map (sampled at 1.25mm isotropic voxel size) was created using the new attenuation map, now well registered to the 60- to 90-minute PET data. PET data were reconstructed using 3D ordinary Poisson ordered-subset expectation maximization reconstruction, with corrections applied for attenuation, scatter, random events, dead-time, sensitivity, and normalization.

To account for global signal differences across subjects, SUV maps were normalized by a pseudoreference region (normalized SUV [SUVR]) with mean SUV in MS around the mean of SUV in controls. Due to MS being a diffuse disease that lacks an anatomically consistent reference region, we used a cluster-based approach. Using FreeSurfer and FSL, we

TABLE 1. Participants' Demographic, Clinical, and MRI Characteristics

Characteristic	Controls, n = 14	All MS, n = 27	SPMS, n = 15	RRMS, n = 12
Demographics and clinical data				
Gender, F/M	6/8	21/6	11/4	10/2
Age, yr, mean (SD)	48 (13)	48 (10)	52 (7)	43 (10)
HAB/MAB	7/7	16/11	10/5	6/6
EDSS, median [range]	—	4 [1–7.5]	6.5 [2–7.5]	2 [1–6]
SDMT, mean (SD)	—	−0.4 (1.8)	−1.4 (1.4)	0.9 (1.3)
Information processing, mean (SD)	—	−0.9 (2.1)	−1.9 (1.9)	0.3 (1.8)
Executive function, mean (SD)	—	−1.3 (2.3)	−2.0 (2.6)	−0.3 (1.5)
Learning recall, mean (SD)	—	−0.4 (1.3)	−0.70 (1.30)	−0.05 (1.2)
Disease duration, yr, median [range]	—	7 [1–40]	21 [6–40]	2 [1–33]
Subjects with at least 1 cognitive test with z score ≤ -1.5	—	20	13	7
Subjects with mild/moderate depression	—	3/4	2/2	1/2
MS treatments				
Dimethyl fumarate	—	6	2	4
Natalizumab	—	5	3	2
Glatiramer acetate	—	4	2	2
β-Interferons	—	2	0	2
Rituximab	—	2	2	0
Fingolimod	—	1	1	0
Teriflunomide	—	1	0	1
None	—	6	5	1
MRI metrics				
WM lesion volume, cm^3, mean (SD)	—	8.1 (11.5)	12.6 (13.8)	2.6 (3.3)
Cortical thickness, mm^2, mean (SD)	2.39 (0.11)	2.33 (0.08)[a]	2.32 (0.10)[a]	2.36 (0.06)
Thalamic fraction[b]	$6.1\ (0.9) \times 10^{-3}$	$5.5\ (1.1) \times 10^{-3}$	$5.2\ (0.9) \times 10^{-3a}$	$5.9\ (0.1) \times 10^{-3}$
Hippocampal fraction[b]	$2.8\ (0.6) \times 10^{-3}$	$2.7\ (0.7) \times 10^{-3}$	$2.5\ (0.6) \times 10^{-3}$	$2.9\ (0.8) \times 10^{-3}$
Intracortical lesions, No. [range]	—	10 [2–69]	20 [3–69]	5 [2–32]
Leukocortical lesions, No. [range]	—	4 [1–151]	4 [1–151]	5 [1–7]
All cortical lesions, No. [range]	—	13 [1–171]	16 [1–171]	8 [3–39]

Beck Depression Inventory–II scores for mild depression = 14–19; for moderate depression = 20–28.

[a] $p < 0.05$ by Mann–Whitney U test.

[b] Thalamic or hippocampal volume/total intracranial volume (SD).

EDSS = Expanded Disability Status Scale; F = female; HAB = high-affinity binders; M = male; MAB = mixed-affinity binders; MRI = magnetic resonance imaging; MS = multiple sclerosis; RRMS = relapsing–remitting MS; SD = standard deviation; SDMT = Symbol Digit Modalities Test; SPMS = secondary-progressive MS; WM = white matter.

identified clusters (minimum size = 9 contiguous voxels) in the WM of controls and NAWM of patients that were within ±0.5 SD of the mean ^{11}C-PBR28 SUV for the global WM in controls. This process was conducted separately for high- and mixed-affinity binders. In MS, NAWM was defined by subtracting WM lesions from the global WM mask. To exclude in patients the presence of microstructural changes due to inflammation[31] in the pseudoreference region, mean diffusivity values in the selected NAWM clusters were compared to mean diffusivity values in WM clusters from controls using linear regression, and covarying for age, and no significant differences were found ($MS = 6.1 \pm 0.5 \times 10^{-10}$ m^2/s; $controls = 6.3 \pm 0.5 \times 10^{-10}$ m^2/s).

In each subject, masks of NAWM, WM lesions, and deep GM were registered to SUVR maps using FNIRT/FSL to extract mean SUVR. For deep GM structures, left and right SUVR were averaged together. To minimize partial volume effects due to the thin and circumvolved nature of cortex, SUVR in the cortex and/or cortical lesions (intracortical, leukocortical) were assessed using a surface-based approach. Using FreeSurfer, as previously detailed,[18] in each subject, whole cortex and cortical lesion (intracortical, leukocortical) SUVR maps were registered onto their corresponding 3T cortical surface, thus resulting in 2D cortical maps. Mean SUVR was computed in each map at midcortical depth.

^{11}C-PBR28 V_T. PET data were binned into 28 time frames (durations: 8×10, 3×20, 2×30 seconds, and 1×1, 1×2, 1×3, 8×5, 4×10 minutes), and dynamic PET images were reconstructed following the same procedure detailed above.

Plasma activity and radioactivity were fitted to a 3-exponential model to derive an input function for the radiotracer injection. The resulting metabolite-corrected plasma input function, and time–activity curves data extracted from the same regions selected for SUVR analyses, were used to fit a 2-tissue compartment model of radiotracer binding and calculate V_T for each region Pixel-wise modeling software (PMOD v3.3) from the rate constant, as previously described.[32,33]

To account for (1) global signal differences across subjects and (2) intersubject variability in the input function,[34] V_T were normalized by the same pseudoreference region (normalized volume of distribution [DVR]) used for SUV. No significant differences in V_T were found between MS subjects and controls in the pseudoreference region.

Statistical Analysis

Statistical analysis was performed using R Statistics software (v2.3). Demographics and conventional MR metrics were compared in MS versus controls using Mann–Whitney *U* test. Linear regression models were used to: (1) compare, in MS versus controls, SUVR and DVR across GM (cortical lesions, whole cortex, deep GM) and WM (lesions, NAWM); (2) investigate in MS the relationship between SUVR and clinical (EDSS, cognitive scores) and structural MRI (cortical thickness, subcortical volume fractions) metrics; and (3) determine the relationship between SUVR and DVR. Age and TSPO affinity were included as covariates of no interest when appropriate. A correction for multiple comparisons was performed using the Holm method with a significance threshold of $p < 0.05$ for each subset of analyses including (1) SUVR and (2) DVR

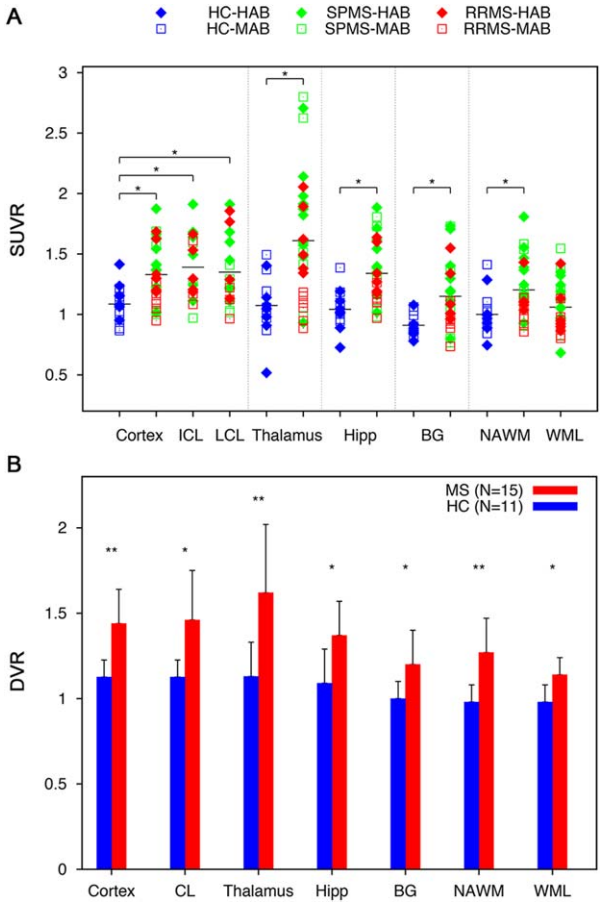

FIGURE 1: (A) Mean normalized ^{11}C-PBR28 standardized uptake values (SUVR) in healthy controls (HC; n = 14) and multiple sclerosis (MS) patients (n = 27) with either relapsing–remitting MS (RRMS; n = 12) or secondary-progressive MS (SPMS, n = 15) across different tissue compartments in gray and white matter. Horizontal bars indicate group averages for high-affinity binder (HAB) and mixed-affinity binder (MAB). Connector lines connect brain tissue compartments that were compared in the whole MS cohort relative to controls using linear regression and covarying for age and affinity binding. In MS, mean SUVR in intracortical and leukocortical lesions were compared with mean cortical SUVR from controls. The asterisks denote when the specific comparison (connector line) between healthy controls and MS patients was statistically significant. (B) Histogram showing mean ^{11}C-PBR28 normalized volumes of distributions (DVR) and standard deviations in different brain regions for both MS subjects (n = 15) and controls (n = 11). ^{11}C-PBR28 DVR were significantly increased in MS subjects compared to controls in all regions assessed. DVR cortical lesion analysis was performed in 9 MS patients. *$p < 0.05$, **$p < 0.005$, by linear regression, adjusting for binding genotype and age, and corrected for multiple comparisons. BG = basal ganglia; CL = cortical lesions; Hipp = hippocampus; ICL = intracortical lesions; LCL = leukocortical lesions; NAWM = normal-appearing white matter; WML = white matter lesions.

TABLE 2. Corrected Probability Values, ES (Cohen *d*), and SE for Comparisons by Linear Regression (Covarying for Age and Binding Affinity) of ^{11}C-PBR28 Uptake across Different Brain Tissue Compartments in MS Subjects versus Controls

	MS vs Controls			SPMS vs Controls			RRMS vs Controls		
Compartment	***p***	**ES[a]**	**SE**	***p***	**ES[a]**	**SE**	***p***	**ES[a]**	**SE**
SUVR	n = 27 vs 14			n = 15 vs 14			n = 12 vs 14		
Cortex	0.007	0.9	0.06	0.01	1.3	0.08	0.1	0.8	0.07
NAWM	0.02	0.9	0.07	0.01	1.3	0.08	0.5	0.5	0.07
WML	0.4	0.3	0.07	0.2	0.6	0.08	0.9	0.1	0.07
ICL	0.007	1.4	0.06	0.01	1.6	0.09	0.04	1.4	0.08
LCL	0.02	1.1	0.07	0.02	1.2	0.08	0.1	1.1	0.1
Thal	0.008	1.2	0.1	0.002	1.7	0.2	0.3	0.9	0.1
Hipp	0.006	1.3	0.06	0.003	1.6	0.09	0.1	1.1	0.07
BG	0.02	1.0	0.06	0.01	1.3	0.09	0.3	0.8	0.07
DVR	n = 15 vs 11			n = 10 vs 11			n = 5 vs 11		
Cortex	0.0007	1.5	0.07	0.005	1.7	0.09	0.03	1.5	0.07
NAWM	0.001	1.5	0.07	0.004	1.6	0.09	0.1	1.3	0.09
WML	0.05	0.9	0.07	0.05	1.1	0.08	1	0.3	0.06
CL[b]	0.02	1.5	0.1	0.03	3.1	0.1	0.03	1.5	0.07
Thal	0.005	1.3	0.1	0.004	1.9	0.1	0.7	0.8	0.1
Hipp	0.04	1.1	0.1	0.05	1.2	0.1	1	0.8	0.07
BG	0.02	1.1	0.07	0.02	1.4	0.07	0.9	0.5	0.06

[a]The ES was computed by adjusting the calculation of the pooled standard deviation with weights for the sample size.
[b]SPMS, n = 6; RRMS, n = 3.
BG = basal ganglia; CL = cortical lesions; DVR = normalized volume of distributions; ES = effect size; Hipp = hippocampus; ICL = intracortical lesions; LCL = leukocortical lesions; MS = multiple sclerosis; NAWM = normal-appearing white matter; RRMS = relapsing–remitting MS; SE = standard error; SPMS = secondary-progressive MS; SUVR = normalized standardized uptake values; Thal = thalamus; WML = white matter lesions.

comparisons in all MS, (3) SUVR and (4) DVR comparisons in MS subgroups relative to controls, (5) correlations between SUVR and DVR, (6) correlations between SUVR and EDSS, (7) information-processing speed, (8) memory functions and, (9) structural data. The standardized effect size (Cohen *d*) was also calculated.

SURFACE-BASED ANALYSIS. Each individual 2D SUVR cortical map, sampled at midcortical depth, was smoothed along the surface with a 10mm full-width at half-maximum Gaussian kernel and normalized to a common template in FreeSurfer. A general linear model was used to assess vertexwise across the entire cortex: (1) differences in ^{11}C-PBR28 SUVR between MS and controls and (2) the relationship in MS between ^{11}C-PBR28 SUVR and clinical scores (EDSS, cognitive scores). Binding affinity, age, and cortical thickness at the vertex level were used as covariates of no interest. Correction for multiple comparisons was performed using Monte Carlo simulation with 10,000 iterations and a significance level of $p < 0.05$. Localization of significant cortical clusters was performed using the Desikan–Killiany atlas in FreeSurfer.

Results

Demographics, Clinical Data, and Conventional MRI Findings

Subjects' demographics, binding genotype, MRI, and clinical data are reported in Table 1. Age was not statistically different between patients and controls.

Mean cortical thickness was lower in all MS and SPMS subjects than in controls. There were no differences in deep GM fractions; only SPMS cases showed significant thalamic atrophy (see Table 1).

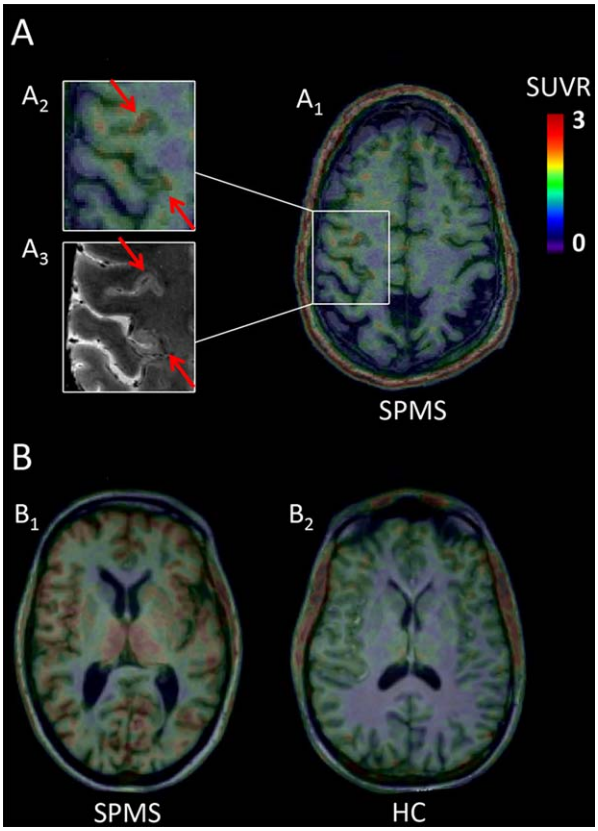

FIGURE 2: (A) Fused magnetic resonance and positron emission tomography (MR-PET) images in a subject with secondary-progressive multiple sclerosis (SPMS) and a high-affinity binding (HAB) genotype (A_1) showing cortical areas of increased ^{11}C-PBR28 standardized uptake values normalized by a pseudoreference region (SUVR). (A_2) Detail of cortical lesions visible on the 3T anatomical scan fused with SUVR images and (A_3) on the coregistered 7T T_2^* images. (B) Fused ^{11}C-PBR28 SUVR MR-PET images in an HAB MS subject (B_1) and in an HAB age-matched healthy control (HC; B_2) showing increased ^{11}C-PBR28 SUVR uptake in the thalamus of the patient.

^{11}C-PBR28 Binding

TSPO LEVELS IN GM. Figure 1A shows ^{11}C-PBR28 SUVR distribution across brain regions in controls and MS subjects, according to their binding genotype. DVR comparisons between MS and controls are illustrated in Figure 1B. Table 2 reports significant differences between groups, and their effect size. Relative to controls, MS cases showed increased ^{11}C-PBR28 SUVR in the whole cortex (23%), thalamus (50%), hippocampus (28%), and basal ganglia (26%). Thalamic lesions were observed in 12 patients (9 SPMS, 3 RRMS), but not in other deep GM structures. Thalamic lesions' SUVR did not differ from uptake in normal-appearing thalamus (paired *t* test).

Twenty MS subjects (SPMS = 12, RRMS = 8) had visible cortical lesions on 7T scans (see Table 1). In 2 patients no cortical lesions could be detected, and in 2 participants 7T images were discarded due to gross motion artifacts. Relative to controls' cortex, ^{11}C-PBR28 SUVR were increased by 28% in intracortical lesions and by 24% in leukocortical lesions. Increased ^{11}C-PBR28 uptake in cortical lesions did not differ significantly from that in normal-appearing cortex (paired *t* test).

The ^{11}C-PBR28 DVR were significantly increased in MS (n = 15) relative to controls (n = 11) in the whole cortex (30%), thalamus (44%), hippocampus (25%), and basal ganglia (19%; see Fig 1B, Table 2). Cortical lesion DVR were also significantly increased (29%) relative to controls' cortex in MS patients (n = 9). Due to the small number of cases with both cortical lesions and blood data, cortical lesion DVR were assessed by grouping intracortical and leukocortical lesions.

Figure 2 illustrates examples of MS cortical lesions on 7T scans that colocalized with areas of increased ^{11}C-PBR28 uptake on fused MR-PET images, and of diffuse thalamic increased tracer binding in MS.

TSPO LEVELS IN WM. Higher TSPO levels were found in MS NAWM relative to control WM (see Fig 1, Table 2), with a 20% increase in SUVR, and a 29% increase in DVR. For WM lesions, we found a modest increase (7%) in ^{11}C-PBR28 SUVR, and higher TSPO levels could be detected in ^{11}C-PBR28 DVR (15%).

TSPO LEVELS IN RRMS AND SPMS. Corrected probability values and effect sizes for comparisons of ^{11}C-PBR28 SUVR and DVR in each MS subgroup relative to controls are reported in Table 2. RRMS showed significant ^{11}C-PBR28 increases in intracortical lesions and whole cortex. SUVR were also increased in thalamus, and hippocampus by ~29 to 22%, although at an uncorrected significance level. SPMS showed significantly increased SUVR and DVR in the whole cortex (28%, 32%), cortical lesions (ranging from 24% to 36%), thalamus (64%, 58%), hippocampus (33%, 30%), and basal ganglia (34%, 25%). SUVR and DVR were increased by 27% and 32% in NAWM. Increased ^{11}C-PBR28 uptake in WM lesions was significant only for DVR (21%).

ASSOCIATION BETWEEN SUVR AND DVR THROUGHOUT THE BRAIN. In all 15 MS subjects (7 with high-affinity and 8 with mixed-affinity binding) and in 11 controls (5 with high-affinity and 6 with mixed-affinity binding) with blood data, there was a positive correlation between SUVR and DVR across all brain tissue compartments (Fig 3).

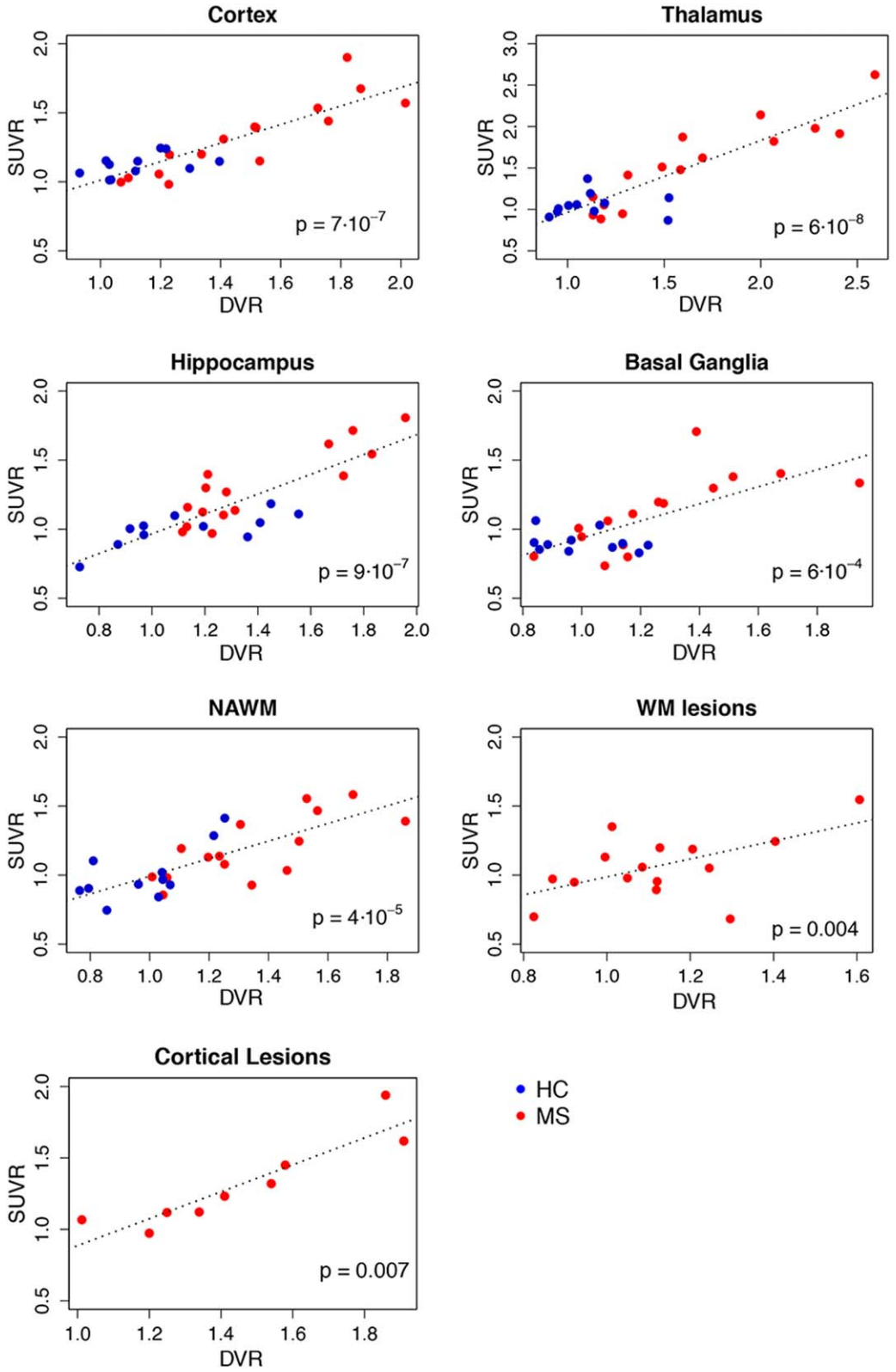

FIGURE 3: Plots illustrating, in the whole study cohort, the correlation between ^{11}C-PBR28 normalized volume of distributions (DVR) and standardized uptake values (SUVR) across different brain tissue compartments by linear regression, adjusting for binding genotype and correcting for multiple comparisons. HC = healthy controls; MS = multiple sclerosis; NAWM = normal-appearing white matter; WM = white matter. [Color figure can be viewed at wileyonlinelibrary.com]

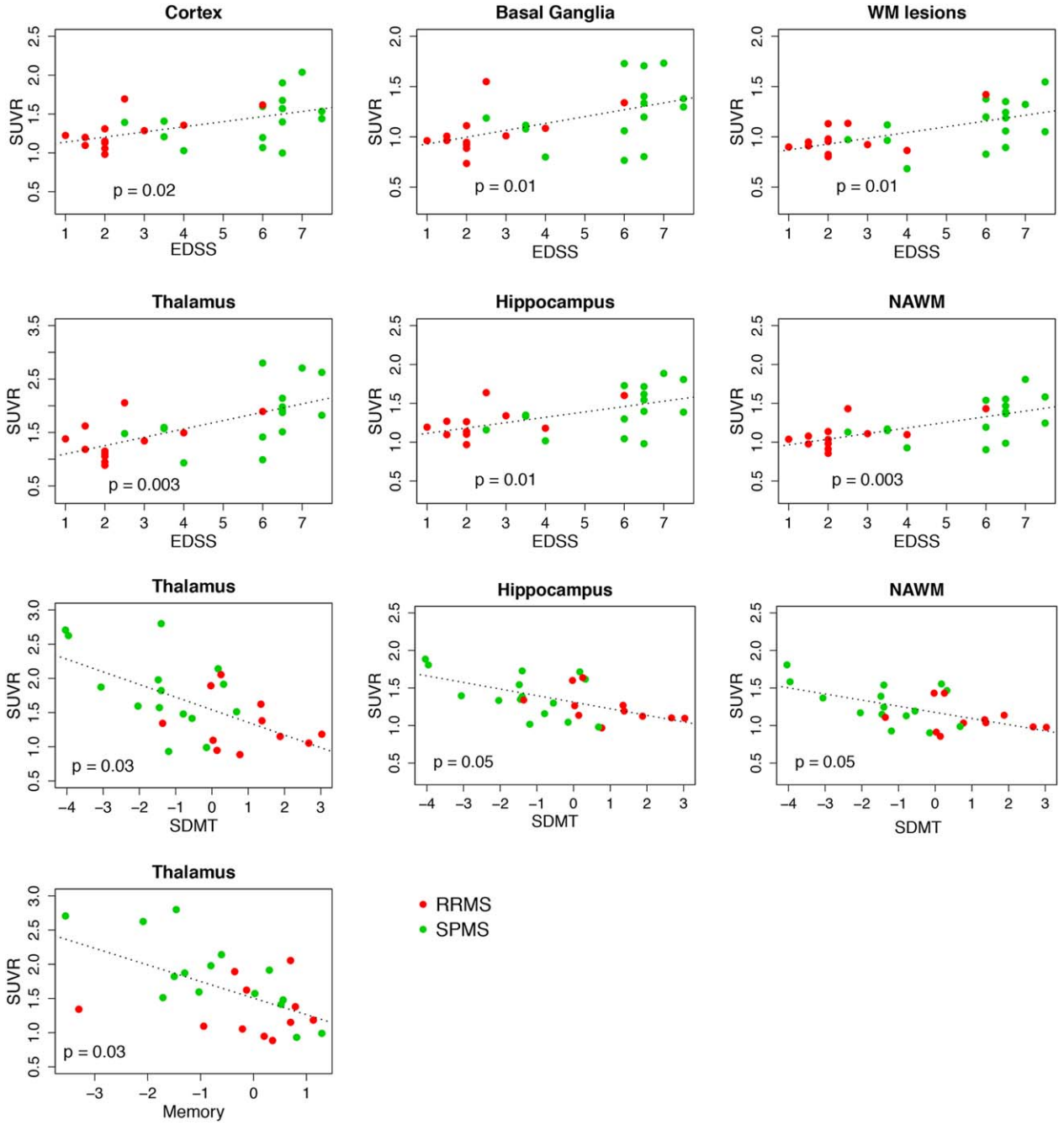

FIGURE 4: Plots illustrating, in the whole multiple sclerosis (MS) cohort, correlations between ^{11}C-PBR28 normalized standardized uptake values (SUVR) and neurological disability and cognitive test scores (linear regression analysis, adjusting for binding genotype and age; all probability values are corrected for multiple comparisons). EDSS = Expanded Disability Status Scale; NAWM = normal-appearing white matter; RRMS = relapsing–remitting MS; SDMT = Symbol Digit Modalities Test; SPMS = secondary-progressive MS; WM = white matter. [Color figure can be viewed at wileyonlinelibrary.com]

Correlation with Clinical and Structural MRI Data

In the MS cohort, EDSS correlated positively with increased ^{11}C-PBR28 SUVR in the whole cortex, thalamus, hippocampus, and basal ganglia. A positive association was also found with ^{11}C-PBR28 uptake in the NAWM and WM lesions (Fig 4).

Impaired memory function scores were associated with increased TSPO levels in the thalamus, whereas we did not find any association with information-processing speed function obtained by averaging SDMT and Trails A scores. Looking at individual tests, we found that SDMT z scores negatively correlated with ^{11}C-PBR28 SUVR in thalamus, hippocampus, and NAWM (see Fig

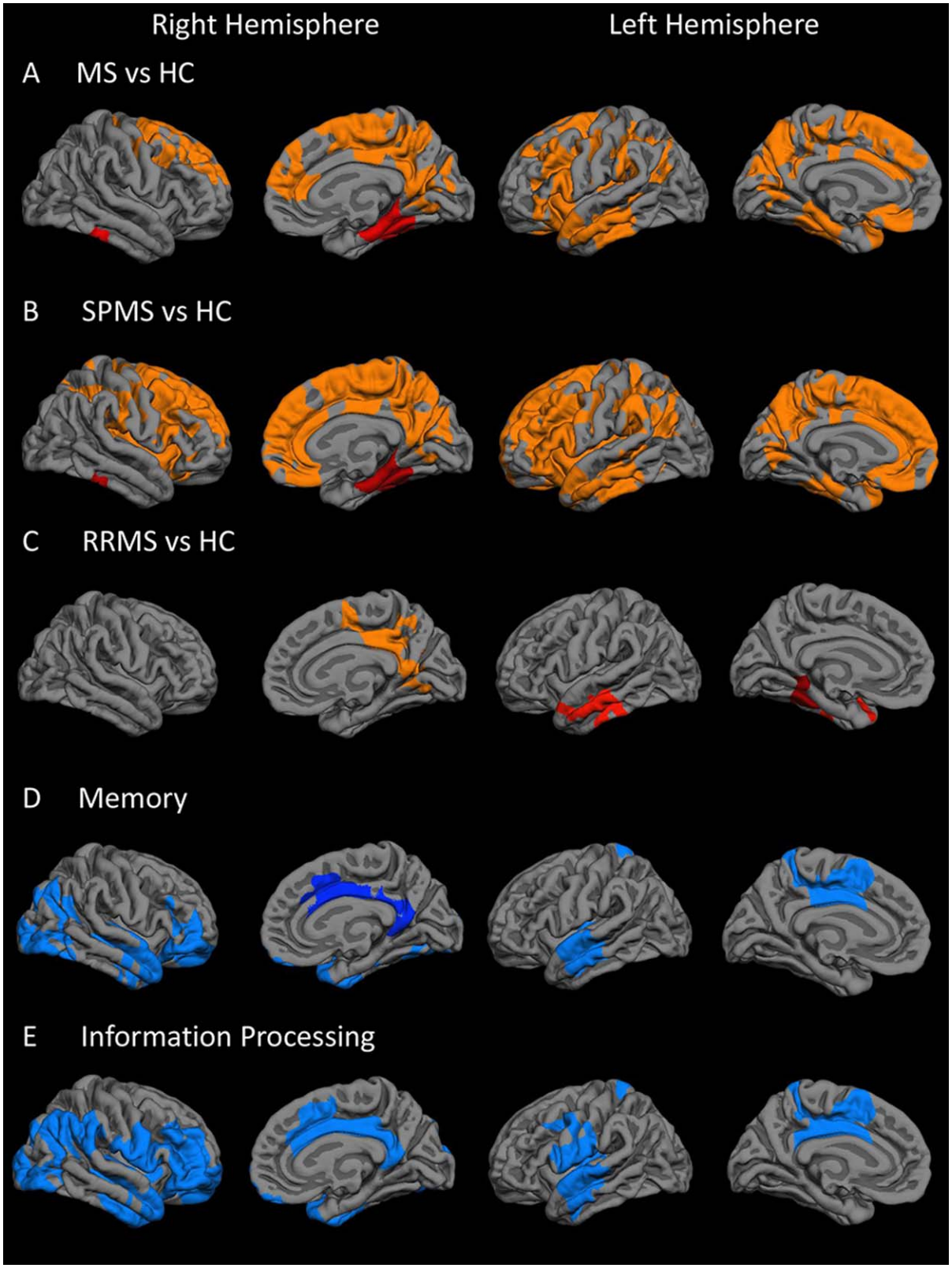

FIGURE 5: (A–C) Overlay of the general linear model significance maps ($p < 0.05$, corrected for multiple comparisons, adjusting for age, binding genotype, and cortical thickness) on the average pial surface showing, relative to healthy controls (HC; n = 14), regions of increased ^{11}C-PBR28 normalized standardized uptake values (A) in the whole multiple sclerosis (MS) cohort (n = 27), as well as (B) in the secondary-progressive MS (SPMS; n = 15) and (C) in the relapsing–remitting MS (RRMS; n = 12) subgroups. (D, E) Regions in all MS cases where ^{11}C-PBR28 uptake correlated negatively ($p < 0.05$, corrected for multiple comparisons) with (D) memory and (E) information-processing speed function.

TABLE 3. FreeSurfer Surface-Based Analysis of Cortical ^{11}C-PBR28 Normalized Standardized Uptake Values

	Hemisphere	Surface Area, mm^2	Corrected p	Area of Peak p for Between-Group Differences
All MS vs controls	Right	2,444	0.002	Parahippocampal
		16,281	0.0001	Precuneus
		1,602	0.04	Superior parietal
		1,772	0.02	Lateral orbitofrontal
	Left	33,578	0.0001	Supramarginal
RRMS vs controls	Right	3,707	0.000	Pericalcarine
	Left	1,725	0.009	Fusiform
		2,362	0.001	Inferior temporal
SPMS vs controls	Right	1,725	0.009	Fusiform
		2,362	0.001	Inferior temporal
	Left	47,009	0.000	Postcentral

	Hemisphere	Surface Area, mm^2	Corrected p	Area of Peak p for Correlation with Cognitive Scores
Memory, CVLT-II–BVMT-R	Right	2,406	0.001	Isthmus cingulate
		5,131	0.0001	Temporal pole
		4,444	0.0001	Lateral orbitofrontal
		6,360	0.0001	Lateral occipital
	Left	3,597	0.0001	Paracentral
		3,059	0.0001	Superior temporal
Information processing, SDMT–Trails A	Right	14,902	0.0001	Inferior parietal
		3,507	0.0001	Posterior cingulate
		10,460	0.0001	Precentral
		6,888	0.0001	Superior temporal
	Left	3,904	0.0001	Superior frontal

BVMT-R = Brief Visuospatial Memory Test–Revised; CVLT-II = California Verbal Learning Test–II; MS = multiple sclerosis; RRMS = relapsing–remitting MS; SDMT = Symbol Digit Modalities Test; SPMS = secondary-progressive MS; Trails = Trail Making Test.

4). There was no association between ^{11}C-PBR28 uptake and executive function.

In all patients and in each MS subgroup, cortical thinning was associated with increased TSPO levels in the thalamus ($p < 0.05$ corrected, covarying for age and binding affinity). In SPMS only, cortical thinning also correlated with neuroinflammation in the cortex and NAWM, although at an uncorrected significance level.

Surface-Based Analysis of Cortical ^{11}C-PBR28 Binding

The cortical surface-based analysis revealed several clusters of increased ^{11}C-PBR28 SUVR in both hemispheres in the entire MS cohort versus controls (Fig 5A–C, Table 3). The increase in ^{11}C-PBR28 cortical uptake was diffuse in SPMS, but more localized in RRMS.

Negative correlations were detected between information-processing speed and memory function and ^{11}C-PBR28 uptake in widespread frontoparietal, temporal, and occipital regions, and right cingulate cortex (see Fig 5D, E, Table 3).

No vertexwise associations were found with executive function or EDSS.

Discussion

Using ^{11}C-PBR28, a second-generation TSPO radiotracer, we demonstrated diffuse microglia/macrophage activation in the cortex, including cortical lesions, and deep GM of MS cases.

Cortical demyelination is a well-established neuropathological feature of MS, and a main substrate of disease progression.[2,4] In histopathological examinations, cortical lesions, particularly in progressive MS, usually

lacked the typical inflammatory features of WM plaques,[2,3] and the prominent cellular population was activated microglia.[2,4]

We used a surface-based analysis to assess, in MS relative to controls, either in cortical lesions imaged with ultra–high-resolution 7T MRI or vertexwise across the whole cortex, differences in TSPO expression sampled at midcortical depth. Compared to volumetric approaches, this method has been shown to improve reliability and detectability of PET cortical signal changes.[35] Previous ^{11}C-PK11195 PET data, using a volume of interest approach, showed increased TSPO levels in MS in frontal, parietal, and occipital cortices.[14] Here, we found that all MS disease stages exhibited abnormally increased TSPO levels, indicative of microglia/macrophage activation, in cortical lesions and several areas of the cortical ribbon. The highest concentration of cortical microglia/macrophage activation was localized in the occipital and temporal cortex in RRMS, the latter often reported as the preferential location for cortical MS demyelination,[36] whereas it extended to widespread frontal and parietal regions in SPMS.

In some neuropathological studies of progressive MS, cortical lesions appeared to be topographically associated with meningeal inflammatory infiltrates, leading to the hypothesis that cortical demyelination may be induced by soluble factors, which diffuse from the meninges into the cortex and trigger demyelination directly or indirectly through microglia activation.[5,37] The extent of meningeal inflammation correlated with microglia activation and the severity of demyelination in the underlying cortex.[4,5] Meningeal inflammation, by means of perivascular lymphocytic infiltration, in association with cortical lesions, has also been described in biopsies at MS onset.[37] The possibility of quantifying in vivo TSPO levels in cortical lesions could provide a tool for assessing the innate immune system inflammatory component of cortical lesions, its severity, and its association with structural cortical integrity. Additionally, it could offer relevant information on the role of microglia/macrophage activation in cortical lesions development at any disease stage. Interestingly, in contrast to WM plaques, RRMS and SPMS showed similarly increased TSPO levels in cortical lesions.

Histopathological findings on the role of inflammation in subcortical GM demyelination and neurodegeneration in MS are sparse and heterogeneous, and variable degrees of inflammation by means of activated microglia/macrophages have been reported in deep GM[7,38] and hippocampus.[7,9] In this study, we showed that microglia/macrophage activation extensively involved the thalamus, hippocampus, and basal ganglia. Previous ^{11}C-PK11195 PET studies reported increased thalamic TSPO levels in MS.[13,15] Abnormally high ^{11}C-PK11195 binding has also been observed in clinically isolated syndrome in the brain central deep GM, although no significant differences were found in any single deep GM structure relative to controls.[39] Here, neuroinflammation in thalamus and deep GM was seen at both disease stages, although more prominently in SPMS.

Our MS cohort showed, relative to controls, significant global cortical thinning, whereas there were no differences in deep GM volumes with the exception of thalamic atrophy in SPMS. Cortical thinning in MS correlated with increased thalamic ^{11}C-PBR28 binding. Increased thalamic ^{11}C-PK11195 uptake secondary to distant cortical pathology has been described in stroke,[40] implying the existence of a "projected neuroinflammatory" response from distant lesions along shared anatomical pathways. The thalami are major hubs in the brain, which integrate and process the signal originating from cortical projections. Spreading of cortical pathology to the thalami, or vice versa, could occur through thalamocortical connections. The direction of such changes could be tested in MS by assessing, longitudinally, microglia/macrophage activation changes along corticothalamic pathways.

The exact relationship between cortical neurodegeneration and locally activated microglia needs to be elucidated. Pathological evidence suggested that, as for cortical lesion development, neurodegeneration may be triggered by meningeal inflammation with cortical microglia activation.[4,5,37] In a series of RRMS and SPMS cases, leptomeningeal inflammation, as seen on postcontrast FLAIR MRI, was found to be associated with more severe cortical atrophy.[41] According to some experimental studies, microglial activation may also constitute a specialized danger signal following neuronal death or injury.[42] In our cohort, however, especially in RRMS, neuroinflammation was not strictly associated with neurodegeneration, suggesting that it might not simply represent an indirect marker or consequence of neuroaxonal loss.

In line with previous observations, we found increased TSPO levels in WM lesions[43,44] and NAWM.[16,43,45] We found that TSPO levels in WM lesions, measured with both SUVR and DVR, were generally lower than those in cortical lesions. Additionally, in RRMS, the highest ^{11}C-PBR28 uptake, relative to controls, was measured in intracortical lesions and focal cortical areas, whereas it was relatively modest in WM. Overall, these observations suggest that the innate immune system–mediated inflammatory events underlying the development of MS lesions might be dissociated

in cortex and WM, especially at earlier disease stages, or there may be more heterogeneity in the inflammatory response associated with WM plaques[46] than with cortical lesions. It is possible, however, that even if 7T MRI was used for cortical lesion detection, some cortical lesions were missed at visual inspection of scans. Nevertheless, cortical lesions identified on 7T T_2^*-weighted images likely represent the areas with greatest cortical demyelination, especially in RRMS.[18]

In our MS cohort, neurological disability correlated with microglial/macrophage activation in deep GM, in addition to neuroinflammation in the cortex and WM as previously reported.[14,16] Here, we also demonstrated that microglia/macrophage activation correlated with reduced cognitive performance in MS. Increased TSPO levels in thalamus, hippocampus, and NAWM were associated with impaired SDMT function, a measure of information-processing speed, which is frequently affected in MS and, thus, commonly evaluated in the clinical setting. Diffusion imaging data highlighted that hippocampal–thalamic–prefrontal disruption affects SDMT performance in RRMS.[47] An association between depression and hippocampal neuroinflammation, as measured by ^{18}F-PBR11, has been recently reported in RRMS.[39] Our study excluded cases with major depression or other psychiatric conditions, and moderate depression was present in only 3 MS patients. Interestingly, in our cohort, information-processing speed dysfunction also correlated with increased ^{11}C-PBR28 binding in frontoparietal, temporal, cingulate, and occipital cortices, in line with previous functional MRI experiments that described large areas of activation in the same cortical regions during SDMT execution.[48] Finally, neuroinflammation in the thalamus, and in widespread temporal and occipital regions, and extending to the cingulate and prefrontal cortex, was associated with decreased memory function as measured by the BVMT-R and CVLT-II, likely reflecting the different neuroanatomical correlates for memory processing of verbal and visual material.

It has been hypothesized that microglia may play a dual role in MS pathogenesis: either detrimental, by causing neuronal dysfunction and promoting oxidative burst, or neuroprotective. Our findings suggest that the prevailing effects, in both GM and NAWM, are detrimental. The observation that SPMS cases showed overall higher brain TSPO levels than RRMS cases further supports this notion. However, it cannot be excluded that, at least at early disease stages, microglia might exert protective functions. Recent data, however, demonstrated that in clinically isolated syndrome persistently increased TSPO levels in NAWM predicted conversion to MS.[16]

We assessed TSPO levels using ^{11}C-PBR28 SUVR and quantitative blood analysis, with both measures showing similar changes in MS. As previously suggested,[34] we used DVR to account for ^{11}C-PBR28 intersubject variability in the input function. Our and previous ^{11}C-PBR28 data[21] seem to suggest that quantitative blood data may be more sensitive than SUVR to microglia/macrophage activation in MS WM lesions, although this needs to be further confirmed. However, the strong positive correlation between SUVR and DVR in all tissue compartments assessed indicates that SUVR estimation is a reliable method for characterizing microglial/macrophage pathology in MS. In humans, ^{11}C-PBR28 SUVR has also been used to reliably distinguish healthy individuals from cases with neurological disorders.[27,49,50] This method is expected to improve subject tolerability by allowing shorter scan time and not requiring arterial catheterization, making it less invasive and more feasible for clinical studies. The use of an integrated MR-PET system further increases patients' compliance, in addition to improving spatial fidelity and registration accuracy.[25]

In this study, we could assess blood–brain barrier integrity with contrast-enhanced MRI only in one-third of MS subjects; thus, we cannot definitely exclude that some of the TSPO changes in the remaining patients were secondary to acute systemic inflammation. However, blood–brain barrier disruption in cortex and deep GM is uncommonly observed in MS using contrast-enhanced MRI,[10,11] and all patients were stable in terms of clinical relapses and MS-related treatments, suggesting that microglia/macrophage activation likely largely reflected chronic inflammation, especially in SPMS.

Microglia could constitute a potential target for monitoring disease course, especially in the compartmentalized inflammation in progressive MS, and the effects of therapies. Our findings could guide longitudinal evaluations in larger MS cohorts to definitely establish the role of neuroinflammation in disease pathogenesis and progression.

Acknowledgment

This study was supported by the Clafin Award; the National Multiple Sclerosis Society (NMSS; RG 4729A2/1); the US Army, Department of Defense (DoD; W81XWH-13-1-0112); an NMSS fellowship (FG-1507-05459; E.H.); the ARSEP Foundation (C.L.); an Italian Multiple Sclerosis Foundation training fellowship (2012/B/04; C.G.); the NIH (1R21NS087472-01A1; M.L.L.); and the DoD (W81XWH-14-1-0543) M.L.L.

We thank G. Arabasz, S. Hsu, and M. Wentworth for their technical and medical assistance with the MR-PET imaging; and F. Turkheimer, M. Veronese, and D. A. Albrecht for their help with quality control of the blood data.

Author Contributions

E.H. and C.G. contributed equally to this work. Conception and design of the study: C.M.; acquisition and analysis of data: all authors; drafting manuscript and/or figures: E.H., C.G., T.G., C.M.

Potential Conflicts of Interest

Nothing to report.

References

1. Zivadinov R, Pirko I. Advances in understanding gray matter pathology in multiple sclerosis: are we ready to redefine disease pathogenesis? BMC Neurol 2012;12:9.
2. Peterson JW, Bo L, Mork S, et al. Transected neurites, apoptotic neurons, and reduced inflammation in cortical multiple sclerosis lesions. Ann Neurol 2001;50:389–400.
3. Bo L, Vedeler CA, Nyland H, et al. Intracortical multiple sclerosis lesions are not associated with increased lymphocyte infiltration. Mult Scler 2003;9:323–331.
4. Magliozzi R, Howell O, Vora A, et al. Meningeal B-cell follicles in secondary progressive multiple sclerosis associate with early onset of disease and severe cortical pathology. Brain 2007;130(pt 4): 1089–1104.
5. Howell OW, Reeves CA, Nicholas R, et al. Meningeal inflammation is widespread and linked to cortical pathology in multiple sclerosis. Brain 2011;134(pt 9):2755–2771.
6. Kooi EJ, Strijbis EM, van der Valk P, Geurts JJ. Heterogeneity of cortical lesions in multiple sclerosis: clinical and pathologic implications. Neurology 2012;79:1369–1376.
7. Haider L, Simeonidou C, Steinberger G, et al. Multiple sclerosis deep grey matter: the relation between demyelination, neurodegeneration, inflammation and iron. J Neurol Neurosurg Psychiatry 2014;85:1386–1395.
8. Geurts JJ, Bo L, Roosendaal SD, et al. Extensive hippocampal demyelination in multiple sclerosis. J Neuropathol Exp Neurol 2007;66:819–827.
9. Dutta R, Chang A, Doud MK, et al. Demyelination causes synaptic alterations in hippocampi from multiple sclerosis patients. Ann Neurol 2011;69:445–454.
10. Calabrese M, Filippi M, Rovaris M, et al. Morphology and evolution of cortical lesions in multiple sclerosis. A longitudinal MRI study. Neuroimage 2008;42:1324–1328.
11. Renard D, Castelnovo G, Campello C, et al. Thalamic lesions: a radiological review. Behav Neurol 2014;2014:154631.
12. Oh U, Fujita M, Ikonomidou VN, et al. Translocator protein PET imaging for glial activation in multiple sclerosis. J Neuroimmune Pharmacol 2011;6:354–361.
13. Banati RB, Newcombe J, Gunn RN, et al. The peripheral benzodiazepine binding site in the brain in multiple sclerosis: quantitative in vivo imaging of microglia as a measure of disease activity. Brain 2000;123(pt 11):2321–2337.
14. Politis M, Giannetti P, Su P, et al. Increased PK11195 PET binding in the cortex of patients with MS correlates with disability. Neurology 2012;79:523–530.
15. Rissanen E, Tuisku J, Rokka J, et al. In vivo detection of diffuse inflammation in secondary progressive multiple sclerosis using PET imaging and the radioligand (1)(1)C-PK11195. J Nucl Med 2014;55:939–944.
16. Giannetti P, Politis M, Su P, et al. Increased PK11195-PET binding in normal-appearing white matter in clinically isolated syndrome. Brain 2015;138(pt 1):110–119.
17. Filippi M, Evangelou N, Kangarlu A, et al. Ultra-high-field MR imaging in multiple sclerosis. J Neurol Neurosurg Psychiatry 2014; 85:60–66.
18. Louapre C, Govindarajan ST, Gianni C, et al. Beyond focal cortical lesions in MS: an in vivo quantitative and spatial imaging study at 7T. Neurology 2015;85:1702–1709.
19. Brown AK, Fujita M, Fujimura Y, et al. Radiation dosimetry and biodistribution in monkey and man of 11C-PBR28: a PET radioligand to image inflammation. J Nucl Med 2007;48:2072–2079.
20. Kreisl WC, Fujita M, Fujimura Y, et al. Comparison of [(11)C]-(R)-PK 11195 and [(11)C]PBR28, two radioligands for translocator protein (18 kDa) in human and monkey: implications for positron emission tomographic imaging of this inflammation biomarker. Neuroimage 2010;49:2924–2932.
21. Park E, Gallezot JD, Delgadillo A, et al. (11)C-PBR28 imaging in multiple sclerosis patients and healthy controls: test-retest reproducibility and focal visualization of active white matter areas. Eur J Nucl Med Mol Imaging 2015;42:1081–1092.
22. Hannestad J, Gallezot JD, Schafbauer T, et al. Endotoxin-induced systemic inflammation activates microglia: [(1)(1)C]PBR28 positron emission tomography in nonhuman primates. Neuroimage 2012; 63:232–239.
23. Owen DR, Yeo AJ, Gunn RN, et al. An 18-kDa translocator protein (TSPO) polymorphism explains differences in binding affinity of the PET radioligand PBR28. J Cereb Blood Flow Metab 2012;32: 1–5.
24. Kurtzke JF. Rating neurologic impairment in multiple sclerosis: an expanded disability status scale (EDSS). Neurology 1983;33:1444–1452.
25. Catana C, van der Kouwe A, Benner T, et al. Toward implementing an MRI-based PET attenuation-correction method for neurologic studies on the MR-PET brain prototype. J Nucl Med 2010; 51:1431–1438.
26. Kolb A, Wehrl HF, Hofmann M, et al. Technical performance evaluation of a human brain PET/MRI system. Eur Radiol 2012;22: 1776–1788.
27. Zurcher NR, Loggia ML, Lawson R, et al. Increased in vivo glial activation in patients with amyotrophic lateral sclerosis: assessed with [(11)C]-PBR28. Neuroimage Clin 2015;7:409–414.
28. Granda ML, Schroeder FA, Borra RH, et al. First D1-like receptor PET imaging of the rat and primate kidney: implications for human disease monitoring. Am J Physiol Renal Physiol 2014;307: F116–F121.
29. van der Kouwe AJ, Benner T, Salat DH, Fischl B. Brain morphometry with multiecho MPRAGE. Neuroimage 2008;40:559–569.
30. Izquierdo-Garcia D, Hansen AE, Forster S, et al. An SPM8-based approach for attenuation correction combining segmentation and nonrigid template formation: application to simultaneous PET/MR brain imaging. J Nucl Med 2014;55:1825–1830.
31. Liu Y, Mitchell PJ, Kilpatrick TJ, et al. Diffusion tensor imaging of acute inflammatory lesion evolution in multiple sclerosis. J Clin Neurosci 2012;19:1689–1694.
32. Gunn RN, Lammertsma AA, Grasby PM. Quantitative analysis of [carbonyl-(11)C]WAY-100635 PET studies. Nucl Med Biol 2000;27: 477–482.
33. Fujita M, Imaizumi M, Zoghbi SS, et al. Kinetic analysis in healthy humans of a novel positron emission tomography radioligand to

image the peripheral benzodiazepine receptor, a potential biomarker for inflammation. Neuroimage 2008;40:43–52.

34. Turkheimer FE, Rizzo G, Bloomfield PS, et al. The methodology of TSPO imaging with positron emission tomography. Biochem Soc Trans 2015;43:586–592.

35. Greve DN, Svarer C, Fisher PM, et al. Cortical surface-based analysis reduces bias and variance in kinetic modeling of brain PET data. Neuroimage 2014;92:225–236.

36. Bo L, Vedeler CA, Nyland HI, et al. Subpial demyelination in the cerebral cortex of multiple sclerosis patients. J Neuropathol Exp Neurol 2003;62:723–732.

37. Lucchinetti CF, Popescu BF, Bunyan RF, et al. Inflammatory cortical demyelination in early multiple sclerosis. N Engl J Med 2011;365:2188–2197.

38. Vercellino M, Masera S, Lorenzatti M, et al. Demyelination, inflammation, and neurodegeneration in multiple sclerosis deep gray matter. J Neuropathol Exp Neurol 2009;68:489–502.

39. Colasanti A, Guo Q, Giannetti P, et al. Hippocampal neuroinflammation, functional connectivity, and depressive symptoms in multiple sclerosis. Biol Psychiatry 2016;80:62–72.

40. Pappata S, Levasseur M, Gunn RN, et al. Thalamic microglial activation in ischemic stroke detected in vivo by PET and [11C]PK1195. Neurology 2000;55:1052–1054.

41. Absinta M, Vuolo L, Rao A, et al. Gadolinium-based MRI characterization of leptomeningeal inflammation in multiple sclerosis. Neurology 2015;85:18–28.

42. Hanisch UK, Kettenmann H. Microglia: active sensor and versatile effector cells in the normal and pathologic brain. Nat Neurosci 2007;10:1387–1394.

43. Colasanti A, Guo Q, Muhlert N, et al. In vivo assessment of brain white matter inflammation in multiple sclerosis with (18)F-PBR111 PET. J Nucl Med 2014;55:1112–1118.

44. Oh U, Fujita M, Ikonomidou VN, et al. Translocator protein PET imaging for glial activation in multiple sclerosis. J Neuroimmune Pharmacol 2011;6:354–361.

45. Debruyne JC, Versijpt J, Van Laere KJ, et al. PET visualization of microglia in multiple sclerosis patients using [11C]PK11195. Eur J Neurol 2003;10:257–264.

46. Lucchinetti C, Bruck W, Parisi J, et al. Heterogeneity of multiple sclerosis lesions: implications for the pathogenesis of demyelination. Ann Neurol 2000;47:707–717.

47. Kern KC, Gold SM, Lee B, et al. Thalamic-hippocampal-prefrontal disruption in relapsing-remitting multiple sclerosis. Neuroimage Clin 2015;8:440–447.

48. Forn C, Belenguer A, Belloch V, et al. Anatomical and functional differences between the paced auditory serial addition test and the symbol digit modalities test. J Clin Exp Neuropsychol 2011;33:42–50.

49. Lyoo CH, Ikawa M, Liow JS, et al. Cerebellum can serve as a pseudo-reference region in Alzheimer disease to detect neuroinflammation measured with PET radioligand binding to translocator protein. J Nucl Med 2015;56:701–706.

50. Loggia ML, Chonde DB, Akeju O, et al. Evidence for brain glial activation in chronic pain patients. Brain 2015;138(pt 3):604–615.